ISIJ International, Vol. 53 (2013), No. 1, pp. 110–118

# Predicting Transient Softening in the Sub-Critical Heat-Affected Zone of Dual-Phase and Martensitic Steel Welds

Elliot BIRO,[1,2] Samuel VIGNIER,[1] Christine KACZYNSKI,[1] Jospeh Robert MCDERMID,[3]* Emmanuel LUCAS,[1] John David EMBURY[2] and Y. Norman ZHOU[4]

1) ArcelorMittal Global Research, 1390 Burlington St., Box 2460, Hamilton, Ont., L8N 3J5, Canada.
2) Dept. of Materials Science and Engineering, McMaster University, 1280 Main St. W., Hamilton, Ont., L8S 4L8, Canada.
3) Dept. of Mechanical Engineering, McMaster University, 1280 Main St. W., Hamilton, Ont., L8S 4L8, Canada.
4) Dept. of Mechanical and Mechatronics Engineering, University of Waterloo, 200 University Ave. W., Waterloo, Ont., N2L 3G1, Canada.

(*Received on July 6, 2012; accepted on September 5, 2012*)

To improve vehicle fuel economy and crash worthiness the automotive industry has been redesigning parts from advanced high strength steels such as dual-phase and martensitic steels. These steels have high strengths with the higher formability characteristics when compared to lower strength conventional steels of similar ductility. These steels derive their unique properties from their complex microstructures containing ferrite and martensite. During assembly welding, the martensite within the sub-critical region of the heat-affected zone tempers, which locally reduces mechanical properties. Although this phenomenon is well studied, it has yet to be quantified. The present work proposes a technique to measure the softening kinetics of dual-phase and martensite steels using rapid isothermal tempering. The resulting model was then validated by predicting the heat-affect zone softening that occurs in laser and resistance spot welds as well as by comparing the microstructures of the rapid tempered samples to the microstructures found in the sub-critical heat-affected zone of welded samples.

KEY WORDS: HAZ softening; laser welding; resistance spot welding; JMAK equation; Avrami equation; dual-phase steel; martensite tempering.

## 1. Introduction

With the environmental issues surrounding the build-up of greenhouse gases and their contribution to global warming, new standards are coming into force requiring the automotive industry to improve the fuel economy of their vehicle fleets.[1] One of the means being chosen by automotive manufacturers to fulfil these regulations is by decreasing vehicle weight. To achieve the necessary weight reductions without compromising passenger safety, conventional low C and high strength low alloy (HSLA) steels commonly used in vehicles ten years ago are being replaced with new higher strength, multiphase advanced high strength steels (AHSS). One of the families of AHSS being adopted for structural applications in significant quantities are the dual-phase (DP) steels.[2]

DP steels have a composite microstructure comprising martensite islands within a ferrite matrix, where the strength of the steel generally increases with increasing volume fractions of martensite.[3] DP steels derive their strength from the interactions between boundary dislocations in the ferrite interacting with the martensite islands, which increases the kinematic hardening contribution to the overall flow stress and their high initial strain hardening rate.[4] This mechanism is one of the primary contributors to the relatively high ultimate tensile strengths (UTS) combined with reasonable uniform elongations characteristic of DP steels as compared to low C and HSLA steels.[5]

However, because the unique mechanical properties of DP steels arise from a multi-phase microstructure containing significant volume fractions of martensite, their mechanical properties will degrade when the martensite is tempered,[6] which occurs in the tempered area of a weldment heat affected zone (HAZ). This phenomenon, known as HAZ softening, was first reported when DP steels were flash butt welded for wheel rim applications.[7,8] In these situations, it was reported that failures were occurring in the softer tempered or sub-critical area of the HAZ.

Since this phenomenon was first observed, some work has been done to characterise it. Xia *et al.* showed that the softening measured within the HAZ of a DP steel weld was a sigmoidal function of the welding heat input and the maximum possible HAZ softening was a linear function of the steel martensite content.[9] Baltazar Hernandez *et al.* showed that in welds exhibiting HAZ softening, only the martensite phase softened and no significant decrease in hardness was observed in the ferrite phase,[10] implying that the observed HAZ softening was solely a product of martensite decomposition. Although this work characterised the mechanisms

* Corresponding author: E-mail: mcdermid@mcmaster.ca
DOI: http://dx.doi.org/10.2355/isijinternational.53.110

of HAZ softening in weldments, the kinetics were not described.

Work has been done to quantify the martensite tempering rate in DP steels using the Johnson-Mehl-Avrami-Kolmogorov (JMAK) equation for both long[11] and short tempering times, the latter using welding data.[12] Both of these studies advanced the literature where the long tempering time study was able to precisely characterise the activation energy for all tempering stages and the welding study demonstrated that the tempering rate increased with martensite C content and was retarded by the presence of carbide-forming alloying elements. However, neither of these approaches were able to provide data that could be used to model HAZ softening. In particular, the long time tempering data did not reflect the welding cycle time scale, where tempering occurs over 0.1–5 s and the welding study did not decouple the effects of temperature and time, meaning that data from this study could not be used to model a generic welding cycle.

The present study seeks to characterise the kinetics of HAZ tempering during the welding cycle by carrying out a series of rapid iso-thermal tempering heat treatments on several DP and martensitic steels. This data will be used to characterise the alloy softening kinetics. This approach will be validated by predicting the HAZ softening observed in laser and resistance spot welds (RSW) made using a range of heat inputs, as well as showing that the microstructures of isothermally tempered DP steels match those found in the non-isothermally tempered (welded) HAZ.

## 2. Methodolgy

The study was carried out on seven steels. Four of these steels had a DP microstructure and three were fully martensitic. All of the steels were industrially produced using the following processing route: casting, hot rolling, cold rolling, annealing and quenching. During the annealing heat treatment, the DP steels were intercritically annealed while the martensitic and hot stamped boron steels were fully austenitized and water quenched. The steels used in this study represent a range of steel chemistries and martensite contents. It should be noted that all of the experimental DP steels had a ferrite-martensite microstructure as opposed to a ferrite-martensite-bainite microstructure. Alloy chemistry, Yurioka carbon equivalent ($CE_N$),[13] martensite volume fraction ($f_{MART}$) (determined by image analysis of scanning electron microscope (SEM) micrographs) and the as-received hardness for all experimental materials may be found in **Table 1**.

Material softening kinetics were characterised by rapid isothermal tempering using a Gleeble 3500 (Dynamic Systems Inc., Poestenkill, NY, USA). All samples were 100 mm × 12 mm with the rolling direction parallel to the long side. During the tempering cycle, samples were heated with average heating and cooling rates of 2 190°C/s and 4 140°C/s, respectively. Sample heating was more consistent than cooling, having standard deviations of 250°C/s and 3 220°C/s, respectively. It should be pointed out that the minimum cooling rate measured was 820°C/s. It is believed that these rates were sufficient to assume an isothermal tempering kinetic. An example of a typical tempering cycle may be seen in **Fig. 1**.

Samples were tempered for times ranging from 0.2 s to 10 s to simulate typical times that the sub-critical HAZ would be at elevated temperature during welding. All experimental tempering temperatures and times are listed in **Table 2**. To determine the minimum tempered hardness of

**Table 1.** Details of experimental materials (chemistry listed in wt%).

| Steel | thickness (mm) | C | Mn | P | S | Si | Cr | Mo | $CE_N$ | $f_{Mart}$ (%) | $T_m$ (°C) | $T_{Ac1}$ (°C) | Base Hardness (HV) | Min Hardness (HV) |
|---|---|---|---|---|---|---|---|---|---|---|---|---|---|---|
| DP780 | 1.5 | 0.10 | 1.8 | 0.01 | 0.01 | 0.31 | 0.02 | 0.02 | 0.31 | 17.5 | 1 516 | 713 | 215.0 | 158.0 |
| DP980-1 | 1.4 | 0.12 | 2.1 | 0.01 | 0.00 | 0.07 | 0.02 | 0.31 | 0.44 | 48.4 | 1 516 | 702 | 307.0 | 190.0 |
| DP980-2 | 1.4 | 0.16 | 1.9 | 0.02 | 0.00 | 0.23 | 0.19 | 0.00 | 0.50 | 56.9 | 1 511 | 712 | 346.0 | 201.0 |
| DP1180 | 1.5 | 0.15 | 1.9 | 0.02 | 0.00 | 0.23 | 0.20 | 0.00 | 0.46 | 76.5 | 1 513 | 713 | 375.0 | 197.0 |
| M190 | 1.8 | 0.18 | 0.4 | 0.01 | 0.00 | 0.19 | 0.03 | 0.00 | 0.26 | 100.0 | 1 517 | 724 | 408.0 | 195.0 |
| M220 | 1.8 | 0.23 | 0.4 | 0.01 | 0.01 | 0.20 | 0.02 | 0.00 | 0.32 | 100.0 | 1 513 | 725 | 478.0 | 200.0 |
| Hot Stamped Boron | 2.0 | 0.23 | 1.2 | 0.01 | 0.00 | 0.28 | 0.20 | 0.00 | 0.43 | 100.0 | 1 508 | 721 | 472.4 | 228.0 |

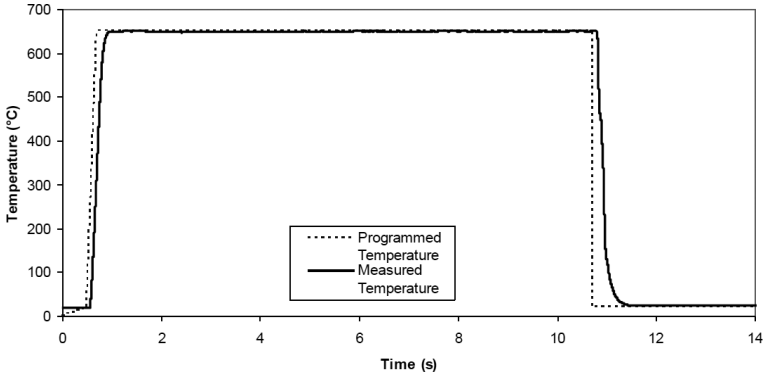


**Fig. 1.** Typical Gleeble heat treatment cycle (taken from a 650°C peak annealing temperature cycle).

**Table 2.** Tempering parameters for experimental steels.

| Temperatures | Times |
|---|---|
| 400°C, 500°C, 600°C, 650°C | 0.2 s, 0.5 s, 1 s, 2 s, 5 s, 10 s, 3 600 s |

each material, all steels were subjected to a 1 hr (3 600 s) furnace temper for all annealing temperatures listed in Table 2. After furnace tempering, samples were immediately water quenched to prevent further alterations to the microstructure.

Microhardness measurements were conducted to monitor the softening of the experimental steels arising from the tempering trials. All hardness measurements presented are the average of between 10–12 measurements taken through the sheet thickness. The large number of data points were intended to smooth the through-thickness hardness variation commonly observed in DP steels.[14] All hardness measurements were performed per ASTM E384-11[15] using a 500 g load with a 15 s dwell time and were spaced more than 2.5 indentation spacings apart. Error bars on the hardness plots represent the 95% confidence interval (CI) of the average hardness value.

Welds were made using both laser and resistance spot welding. Laser welding was carried out using a 4 kW Nd:YAG laser. The spot diameter was approximately 400 $\mu$m and welding speeds were varied between 3–8 m/min. All laser welds were shielded with Ar gas flowing at 30 L/min. Spot welds were made using a 50 Hz AC pedestal welding machine per ISO 18278-2.[16]

Heat input to the work piece from the laser welding process was determined by the method of Xia *et al.*,[9] who calculated it from measurements taken from the weld cross-section using a modified version of Rosenthal's equation for two dimensional heat transfer.[17] As spot welds are axisymmetric, heat input for these welds could not be evaluated using this equation. In this case, the heat input was calculated numerically with SORPAS (SWANTEC Software and Engineering ApS, Lyngby, Denmark) by matching the simulation results with the cross-sectional weld geometry. Minimum hardness values for all welds were taken from hardness maps measured across the weldments. Each map was separated into lines through the sheet thickness and the minimum hardness value on each profile represented the minimum hardness value at the specific depth the hardness profile was measured. All of the hardness values selected (10–18 depending on sheet thickness) were then averaged to determine the minimum hardness value of a particular weld.

Standard transmission electron microscopy (TEM) thin foils were used to examine the microstructure of all samples except for those taken from the low heat input laser weld, where the thin foils were prepared using focused ion beam (FIB). Standard thin foils were ground to between 60–80 $\mu$m using standard metallographic techniques, from which 3 mm diameter TEM sample discs were punched. The samples were thinned by electrolytic jet polishing using a 15°C acetic acid solution with 5% perchloric acid at 70 V with 60 mA. FIB thin foils were cut from a cross-sectioned mount using $Ga^+$ ions. The thin foils were then attached to a Cu grid, thinned using $Ga^+$ ions and cleaned with Ar. All samples were viewed using a Philips CM12 TEM (Royal Philips Electronics, Amsterdam, The Netherlands) at an acceleration voltage of 120 keV. The TEM images presented below are representative of between 5 to 10 imaged areas, depending on the sample, with the exception of the low heat input laser weld where only two areas could be imaged due to the FIB preparation technique. All TEM samples examined were taken from the DP780 grade listed in Table 1.

### 2.1. Softening Kinetics Model

Per the methodology of Biro *et al.*,[12] material softening during isothermal tempering was modeled using the Johnson-Mehl-Avrami-Kolmogorov (JMAK) equation:[18–21]

$$\phi = 1 - \exp\left(-kt^n\right) \quad \text{..... (1)}$$

where $\phi$ represents the fraction of the softening reaction completed, $t$ is time, $n$ is a fitting parameter representing the reaction rate and $k$ is a fitting parameter characterizing the energy barrier to softening. As softening in DP steels is due to martensite tempering,[10,12,22] where the tempering rate is temperature dependant, $k$ was modelled using the Arrhenius equation:

$$k = k_0 \exp\left(\frac{-Q}{RT}\right) \quad \text{..... (2)}$$

where $k_0$ is a fitting parameter, $Q$ is the activation energy for softening, $R$ the universal gas constant and $T$ the absolute temperature. As mentioned above, reaction progress was monitored by changes in material hardness. It is understood this may not be directly proportional to the progress of the tempering reaction, but it is of interest when considering how post-welding HAZ mechanical properties differ from those of the base material. The progress of the softening reaction ($\phi$) was defined as follows:

$$\phi = \frac{H_{BM} - H}{H_{BM} - H_\infty} \quad \text{..... (3)}$$

where $H_{BM}$ is the hardness of the base material, $H$ the measured hardness of the sample at the point of interest, and $H_\infty$ the minimum hardness, defined in the present case as the hardness of the material after tempering 1 hour (3 600 s) at 650°C.

### 2.2. Modelling of Weld Temperature History

During welding the temperature history in the sub-critical HAZ was assumed to be parabolic, per Ion *et al.*[23] This assumption greatly simplified modelling the weld softening. Use of this assumption is believed to be appropriate because the parabolic temperature profile fits the actual welding temperature history very well near its peak temperature, where the majority of the tempering occurs (see **Fig. 2**). The temperature history for each weld was defined as follows:

$$T = \left(T_{Ac_1} - T_0\right)\left[-\left(\frac{t-\tau}{\tau}\right)^2\right] + T_{Ac_1} \quad \text{..... (4)}$$

where $T$ is temperature, $T_{Ac1}$ the alloy $Ac_1$ temperature and $T_0$ the ambient temperature. $\tau$ is a time constant, representing the time for the sub-critical HAZ to heat from ambient temperature to its peak temperature, the $Ac_1$ temperature in this case (see Fig. 2). For the laser welds in this study, $\tau$ was calculated using the equation of Xia *et al.*:[9]

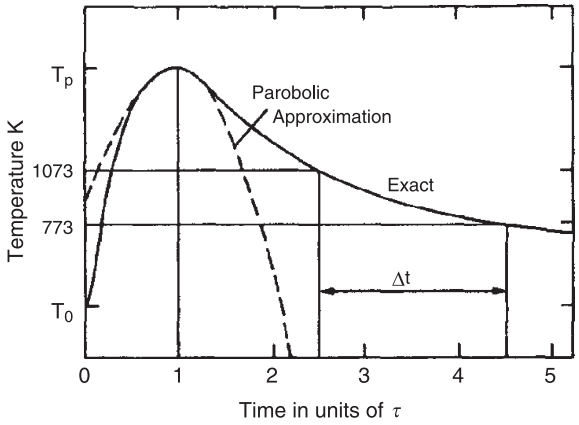


**Fig. 2.** Comparison between the exact temperature history during welding and that of the parabolic temperature history for an arbitrary area within the HAZ (taken from [Ref. 23]).

$$\tau = \frac{\left(Q_{net}/vd\right)^2}{4\pi e \rho c_p \lambda \left(T_{Ac_1} - T_0\right)^2} \quad \text{..... (5)}$$

where $Q_{net}$ is the heat input, $v$ the welding speed, $d$ the sheet thickness, $\rho$ the density of steel (7 860 kg/m$^3$), and $c_p$ and $\lambda$ the steel constant pressure heat capacity (680 J/Kg/K) and thermal conductivity (30 W/m/K), respectively. The normalized heat input ($Q_{net}/vd$) was calculated by determining the heat input necessary to result in the observed distance between the fusion boundary and boundary of the sub-critical HAZ using the Rosenthal equation:

$$Q_{net}/vd = \frac{\rho c_p \left(r_{Ac_1} - r_m\right)\left(2\pi e\right)^{1/2}}{\left(\frac{1}{T_{Ac_1} - T_0} - \frac{1}{T_m - T_0}\right)} \quad \text{..... (6)}$$

where $r_m$ and $r_{Ac_1}$ are the distances measured (taken from weld cross-sections) from the weld centreline to the fusion boundary and the isotherm corresponding to the $Ac_1$ temperature, respectively, and $T_m$ is the melting temperature of the steel. It should be recalled that, because the spot welds are axisymmetric, $\tau$ for these welds was calculated using SORPAS.

## 3. Results and Discussion

### 3.1. Tempering Kinetics Quantification

When the hardnesses of the tempered samples were plotted against their respective tempering times, it was seen that hardness decreased sigmoidally with time in all cases. Furthermore, as would be expected, the hardness of the samples decreased as the tempering temperature increased for similar tempering times. Examples of these general trends are shown for the dual phase DP780 and M220 martensitic steels in **Figs. 3** and **4**, respectively. It should be noted that the increase in hardness above the base metal value seen at short tempering times for the DP780 samples tempered at 400°C was not seen in any of the other samples. As this was unique to the DP780 tempered at 400°C and did not change the sigmoidial nature of the hardness change with tempering time it was not investigated further. When the hardness values were converted to $\phi$ using Eq. (3) and plotted versus tempering time, the softening results took on the classic

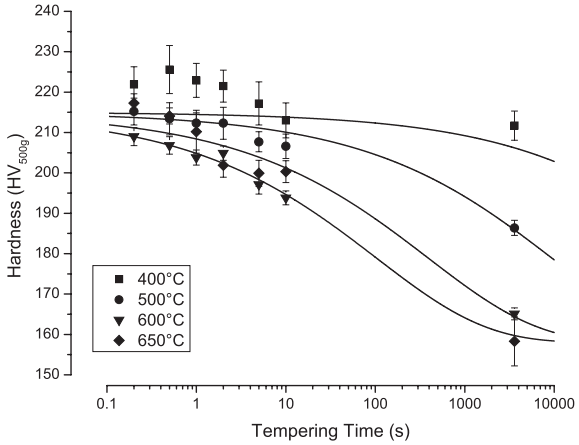


**Fig. 3.** Hardness of tempered DP780 as a function of tempering time and temperature.

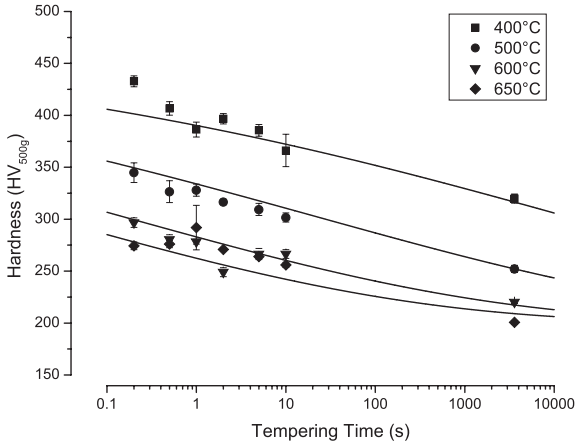


**Fig. 4.** Hardness of tempered M220 as a function of tempering time and temperature.

JMAK form (**Figs. 5** and **6**). It should be noted that only the samples tempered at 650°C approached 1 because of how $\phi$ was defined relative to the reference hardness, $H_\infty$.

All of the softening data were fit to the JMAK equation by standard non-linear regression, the results of which are summarized in **Table 3**. It should be noted that the general goodness-of-fit for the data, as characterized using the adjusted $R^2$ parameter, exceeding 0.9 in all cases except for the DP780 samples, where the $R^2$ value was 0.79 (see Table 3). Although the fits were generally very good, the errors associated with the $k_0$ parameter values were high and in the case of the DP780 sample, the $k_0$ value was not significant (Table 3).

The values fit for Q and n (Table 3) were significantly different from the typical values associated with martensite tempering using the JMAK equation. In general, the literature reports much higher activation energies (177 to 270 kJ/mol)[24–28] for stage III tempering (*i.e.* cementite formation) for the temperature ranges tested in the present case, although a value as low as 82 kJ/mol has been reported.[29] However, it should be noted that the above literature measured the activation energy using dilatometry, which is a more direct measurement of this transformation than the hardness measurements used in this work. When the current activation energies are compared to the results of work that measured tempering progression using hardness measure-

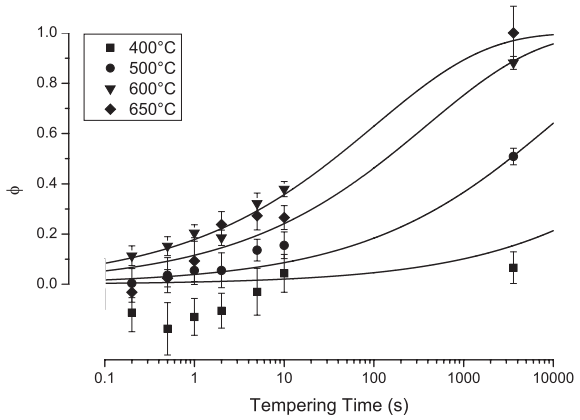


**Fig. 5.** Calculated fraction of softening completed for DP780 as a function of tempering time and temperature.

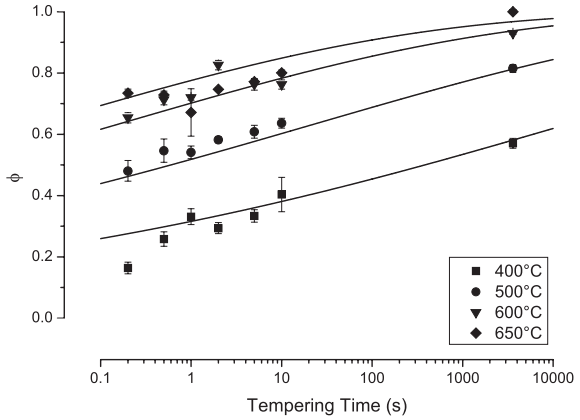


**Fig. 6.** Calculated fraction of softening completed for M220 as a function of tempering time and temperature.

**Table 3.** JMAK fitting parameters and model goodness of fit measurement for experimental steels.

| Steel | Q (kJ/mol) | | $k_0$ | | n | | Adj $R^2$ |
|---|---|---|---|---|---|---|---|
| | Value | *95% CI* | Value | *95% CI* | Value | *95% CI* | |
| DP780 | 62.8 | *13.72* | 700.7 | *1 245.0* | 0.351 | *0.048* | 0.79 |
| DP980-1 | 54.3 | *3.90* | 613.3 | *320.3* | 0.189 | *0.012* | 0.93 |
| DP980-2 | 39.4 | *2.10* | 144.8 | *42.3* | 0.150 | *0.010* | 0.94 |
| DP1180 | 39.2 | *2.02* | 167.7 | *47.7* | 0.139 | *0.010* | 0.94 |
| M190 | 47.9 | *2.61* | 687.0 | *254.2* | 0.151 | *0.013* | 0.95 |
| M220 | 28.3 | *1.39* | 59.9 | *12.4* | 0.101 | *0.009* | 0.94 |
| Hot Stamped Boron | 43.3 | *1.84* | 458.6 | *122.2* | 0.118 | *0.010* | 0.96 |

ments, the current results are more comparable. For example, Takahashi and Bhadeshia[30] measured an activation energy of 33.5 kJ/mol and Holloman and Jaffe[31] measured activation energies ranging from 50 to 209 kJ/mol, depending on the initial hardness of the martensite. It should be further noted that the values of n from the present work do not match the classic JMAK values of 3–4 for spherical particles.[32] However, it should be understood that the use of the JMAK equation in the present case does not represent the conditions under which it was derived, where a daughter phase was nucleated into a parent phase and grew until their transformation was complete. In the case of tempering, carbides are formed and grow until an equilibrium size is reached. The results presented here are agree with Takahashi and Bhadeshia,[30] who also found that the value of n was below 3–4, determining n to be 0.62. However, this value is approximately 2–6 times greater than the values measured in this study. The value of $k_0$ was not compared to literature values because the units are dependent on the value of n.

Although the JMAK parameters presented in this work agree with the data presented from other studies where tempering kinetics were evaluated using hardness measurements,[30,31] it is believed that the values derived for Q and n cannot give any specific insight into the underlying mechanisms responsible for the observed softening. For example, the observed softening can be attributed to a number of processes occurring simultaneously during both the rapid heat treatment and in the HAZ during welding thermal cycles, including martensite tempering (including carbide growth, the effect of alloy chemistry on carbide growth and formation of new ferrite), relaxation of residual stresses and the recovery and recrystallization of deformed grains with its attendant reduction of dislocation density. Thus, it is believed that the present values of the activation energy (Q) and time exponent (n) are actually an apparent activation energy and time exponent which are combinations of all of the above processes. Thus, the apparent disagreement between the values of Q and n with the classic tempering literature, which largely agree with the activation energy for C diffusion, can only be resolved through de-convolution of the terms comprising the derived apparent activation energies and time exponents. This exercise is beyond the scope of the present study and will be addressed in a subsequent contribution.

However, the evidence in Table 3 concerning the goodness-of-fit parameter (adjusted $R^2$) clearly indicates that the present form of the JMAK equation is a convenient mathematical representation of the combined mechanisms leading to the observed the HAZ softening. Furthermore, it can be seen that this mathematical form can be applied across a variety of chemistries and starting martensite contents across this class of alloys and can be used as an empirical predictor of the softening kinetics and material properties in the subcritical HAZ.

### 3.2. Using the JMAK Equation to Describe Non-Isothermal Tempering During Welding

To compare the hardness change during isothermal Gleeble tempering to the non-isothermal tempering cycle found in welds, the tempering damage over the entire welding cycle must be summed. However, because of difficulties associated with integrating the nested exponentials found within Eq. (1) this is very difficult. To overcome this issue, other researchers have changed Eq. (1) such that the term within the exponential became $-(kt)^n$,[25,26] which greatly simplifies the integration. However, this approach was not followed here. Instead, it was decided to convert the thermal history experienced during welding to an equivalent isothermal temperature heat treatment with a tempering temperature equal to the alloy $Ac_1$ temperature (Table 1). This was done by equating Eq. (1) evaluated at the alloy $Ac_1$ temperature to Eq. (1) evaluated at the instantaneous HAZ temperature

during the welding cycle and integrating this expression from $t = 0$ to $t = 2\tau$ (the time for the complete weld cycle). This resulted in the following expression:

$$t_{Ac1} = \int_{t=0}^{t=2\tau} \exp\left[\frac{Q}{Rn}\left(\frac{1}{T_{Ac_1}} - \frac{1}{T}\right)\right] dt \quad \text{..... (7)}$$

where $t_{Ac_1}$ is the equivalent isothermal tempering time at the $Ac_1$ for the subject welding cycle. Although this equation may applied to any general welding cycle, in this study, the parabolic assumption from Fig. 2 was used. Once $t_{Ac_1}$ was calculated, an equivalent $T_{Ac_1}$ isothermal HAZ softening may be predicted using Eq. (1). It is understood that calculating HAZ softening using the isothermal equivalent from Eq. (7) assumes that the final hardness for a tempered material will be temperature independent for long tempering times. From Figs. 3 and 4 this is not certain. However, as Hollomon and Jaffe[31] showed that tempered hardness is a function of a tempering parameter combining the effects of temperature and time and not temperature alone, it is felt that the above assumption is justified considering that $t_{Ac_1}$ is effectively a tempering parameter representing the equivalent tempering time for the welding cycle if it was entirely carried out at the $Ac_1$ temperature.

### 3.3. Predicting the Hardness of Laser and Spot Welds at $r_{Ac_1}$

With the conversion factor to compare the non-isothermal temperature cycles of welding to the isothermal cycle needed for the JMAK equation (Eq. (7)), the hardness at $r_{Ac_1}$ or minimum HAZ hardness ($H$, Eq. (3)) for a given set of welding conditions may be predicted by rearranging Eq. (3) such that:

$$H = H_{BM} - \phi\left(H_{BM} - H_{\infty}\right) \quad \text{..... (8)}$$

To validate whether the proposed JMAK equation could be used to predict the minimum HAZ hardness, a series of high and low heat input laser and resistance spot welds were made from the materials examined in this study. The welding time constants, describing the thermal history of each weld (from Eqs. (4) and (5)), may be found in **Table 4**. Other material properties used in these calculations (*e.g.* base material hardness) can be found in Table 1. The minimum hardness values measured in these welds were then compared to the minimum HAZ hardness predicted using the isothermal $T_{Ac_1}$ annealing time ($t_{Ac_1}$, Eq. (7)). When the predicted and measured hardness values were compared, it was found that the average absolute error was 16.2 ± 5.6 HV, which translates to an error of 6.2 ± 2.1% when normalized against the base material hardness (see **Fig. 7**). These hardness predictions were then subtracted from the base material hardness to predict maximum softening ($H_{BM} - H$), where these results showed stronger agreement with the measured values (**Fig. 8**). It should also be noted that although the absolute error from the hardness predictions appear large, the predicted hardness values were within ±10% of the measured hardness values and are felt to be as accurate as may be reasonably expected within the context of the process variations inherent in the welding process. Thus, these results imply that the data generated through isothermal annealing experiments can be successfully used to predict the HAZ softening characteristics of DP and martensitic steels through proper transformation of the non-isothermal temperature profiles characteristic of welding to the isothermal processes characteristic of those described using the JMAK equation.

**Table 4.** Minimum hardness and time constants of weld samples to validate JMAK softening model (Figs. 7 and 8).

| Steel | Laser Welding | | | | Resistance Spot Welding | |
|---|---|---|---|---|---|---|
| | High Heat Input | | Low Heat Input | | | |
| | $\tau$ (s) | Hardness ($HV_{500\,g}$) | $\tau$ (s) | Hardness ($HV_{500\,g}$) | $\tau$ (s) | Hardness ($HV_{500\,g}$) |
| DP780 | 0.104 | 211 | 0.049 | 216 | 0.650 | 210 |
| DP980-1 | 0.147 | 264 | 0.045 | 267 | 0.820 | 252 |
| DP980-2 | – | – | – | – | 0.640 | 277 |
| DP1180 | – | – | – | – | 0.640 | 275 |
| M190 | 0.063 | 246 | 0.036 | 256 | 0.770 | 236 |
| M220 | 0.058 | 235 | 0.032 | 262 | 0.770 | 238 |
| Hot Stamped Boron | 0.031 | 251 | 0.040 | 261 | 0.770 | 282 |

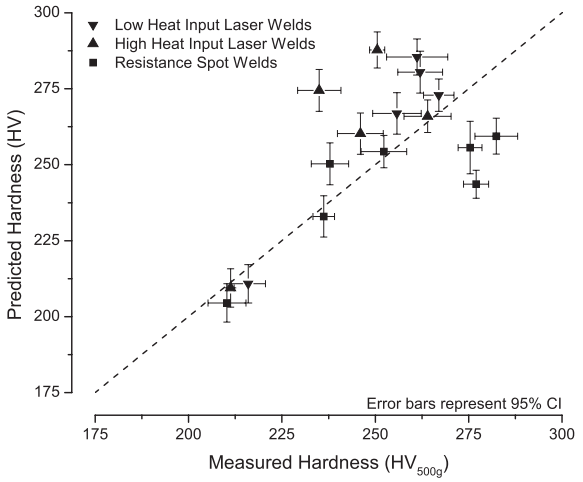


**Fig. 7.** Comparison between the measured hardness and the hardness predicted by the JMAK equation using the parameters listed in Table 3.

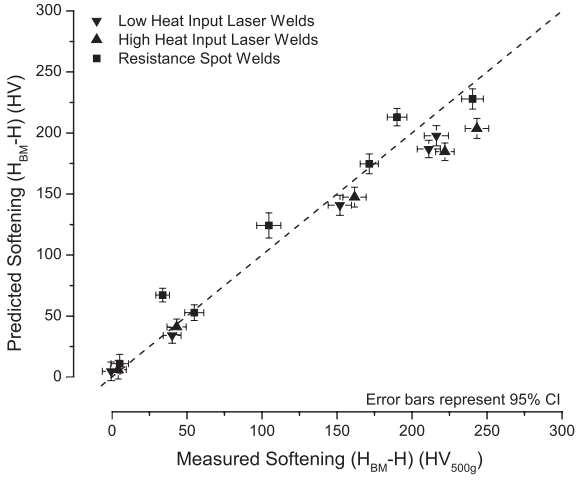


**Fig. 8.** Comparison between the measured HAZ softening and the HAZ softening predicted by JMAK equation using the parameters listed in Table 3.

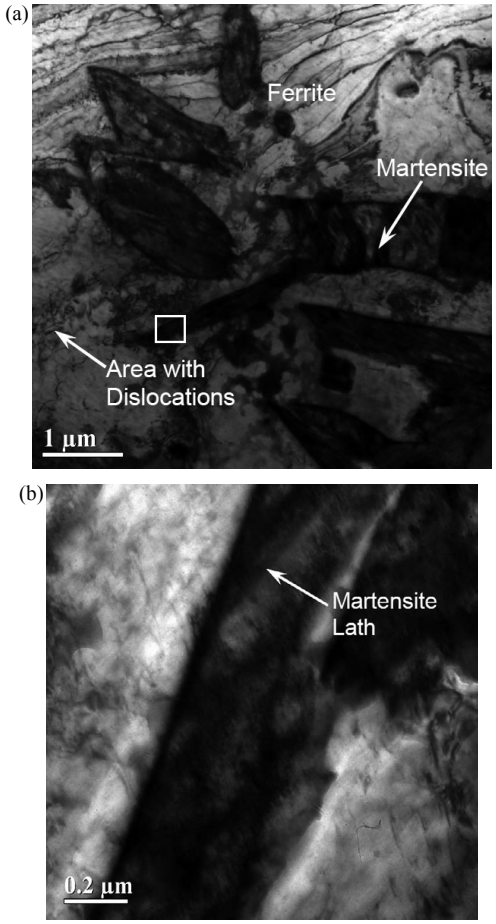


**Fig. 9.** Structure of the as-received DP780 at (a) low and (b) high magnification.

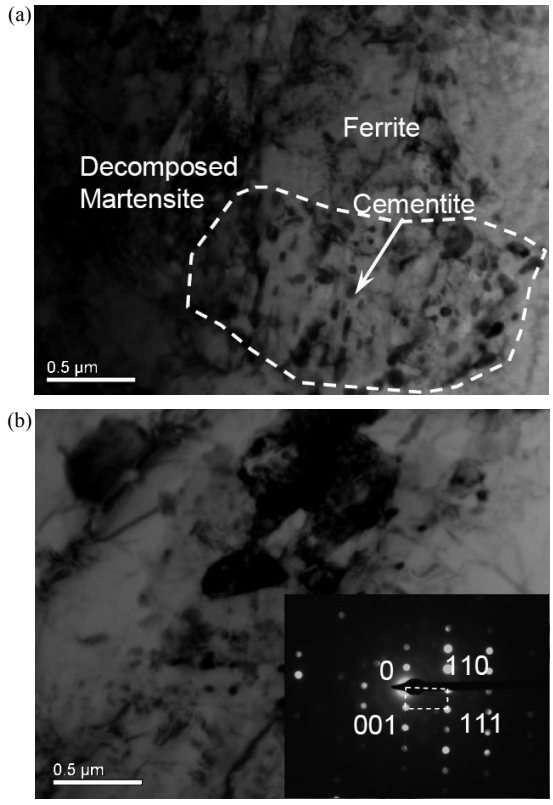


**Fig. 10.** Tempered HAZ of DP780 welded with high heat input showing (a) the decomposed microstructure and (b) an area with large carbides along with the SAD pattern of the carbides found in the decomposed martensite.

### 3.4. Microstructural Comparison of Sub-critical Weld HAZ and Gleeble Samples

Microstructural analysis was carried out to verify that the isothermal tempering treatments produced the same transformations in the experimental steels as the non-isothermal welding tempering cycle which occurs in the sub-critical HAZ. For this purpose, a TEM analysis comparing the sub-critical HAZ of laser welded DP780 using high heat input ($\tau$ = 6.8 s and $t_{Ac_1}$ = 3.0 s) and low heat input ($\tau$ = 0.045 s and $t_{Ac_1}$ = 0.020 s) to Gleeble samples tempered at 650°C for 10 and 0.5 s was carried out. The relative $t_{Ac_1}$ and $\phi$ values for these samples may be compared in **Table 5**. As part of this analysis, the as-received base material was examined,

**Table 5.** Relative $t_{Ac_1}$ and $\phi$ values of samples used for TEM examination.

| Sample | $t_{Ac_1}$ (s) | $\phi$ |
|---|---|---|
| High Heat Input Weld | 3.00 | 0.39 |
| Long Isothermal Tempering Time | 2.24 | 0.36 |
| Low Heat Input Weld | 0.02 | 0.08 |
| Short Isothermal Tempering Time | 0.11 | 0.10 |

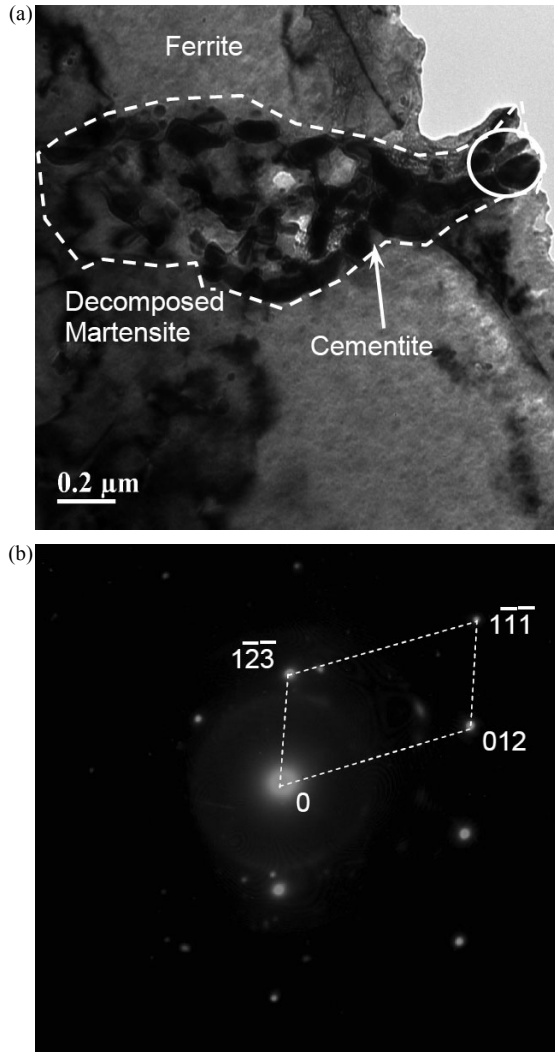


**Fig. 11.** DP780 heat treated in the Gleeble at 650°C for 10 s showing (a) the decomposed microstructure and (b) the SAD pattern of the carbides found in the decomposed martensite from the indicated area.

which revealed the expected mixture of ferrite and martensite as well as the high dislocation density typically associated with DP steel microstructures (**Fig. 9**).

**Figure 10** shows the microstructure of the DP780 sample welded using high heat input (*i.e.* $\tau = 6.8$ s). It can be clearly seen that the martensite had decomposed to ferrite and carbides approximately 50 nm in diameter. It can also be seen that the boundary of the original martensite grain was still visible (Fig. 10). When the Gleeble heat treated samples were viewed (**Fig. 11**), the martensite laths could no longer be discerned and some of the carbide particles had grown to approximately 100 nm in diameter (Fig. 11). This difference is not surprising as the tempering time of the Gleeble tempered sample was almost twice that of the $t_{Ac_1}$ from the welded sample. However, the two samples are similar enough that it may be said that their respective decompositions followed a similar progression as the cementite particle sizes seen in both sample are of the same order of magnitude and the ferrite grains are lacking the dislocations seen in the base material structure.

Although the higher heat input samples were similar, this was not the case for the low heat input samples. The welded sample (**Fig. 12**) appears to be an early state of martensite decomposition. Although decomposed martensite was found, non-decomposed martensite grains were also seen. All of the cementite appears rod-like in shape whereas in the Gleeble tempered sample (**Fig. 13**), all of the martensite decomposed with the cementite clearly forming on the lath boundaries. Also it should be noted that the cementite in the Gleeble samples had already spherodized contrary to what was seen in the welded sample (Fig. 12). The difference between the samples should not be surprising considering that the tempering time of the Gleeble samples was over an order or magnitude larger than the welded samples, which was unavoidable as the Gleeble was not capable of tempering samples as quickly as could be done in the low heat input welds.

Although the Gleeble and weld tempered samples were not comparable in all cases, it was still seen that the samples decomposed to the same products. Furthermore, if the samples are viewed in order of increasing heat input, it may be seen that they all follow the same tempering progression where the martensite decomposed to cementite and ferrite, the cementite spherodized on lath boundaries and finally the cementite coarsened and the underlying martensitic struc-

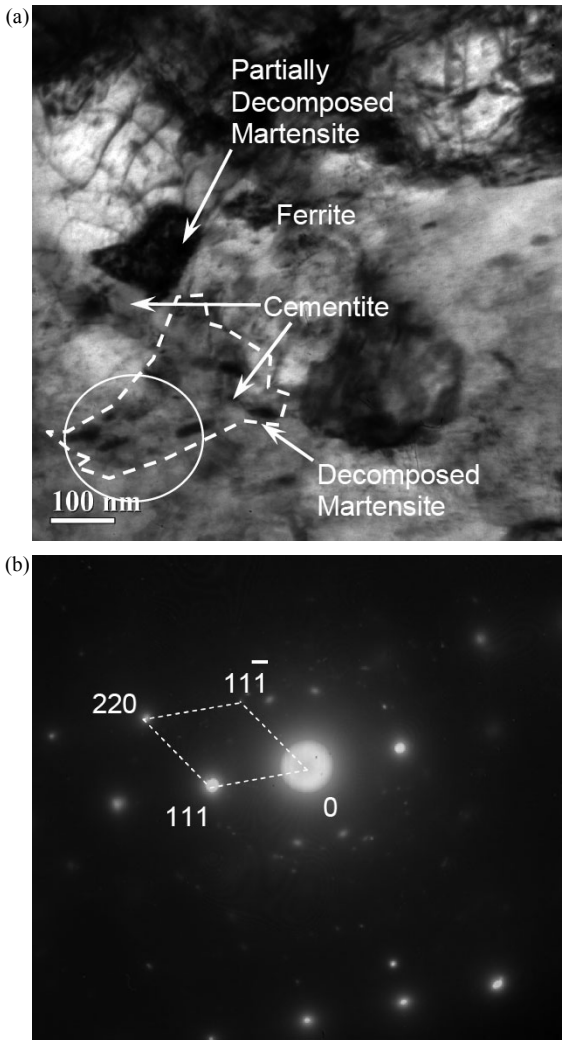


**Fig. 12.** Tempered HAZ of DP780 welded with low heat input showing (a) the partially decomposed microstructure and (b) the SAD pattern of the carbides found in the decomposed martensite.

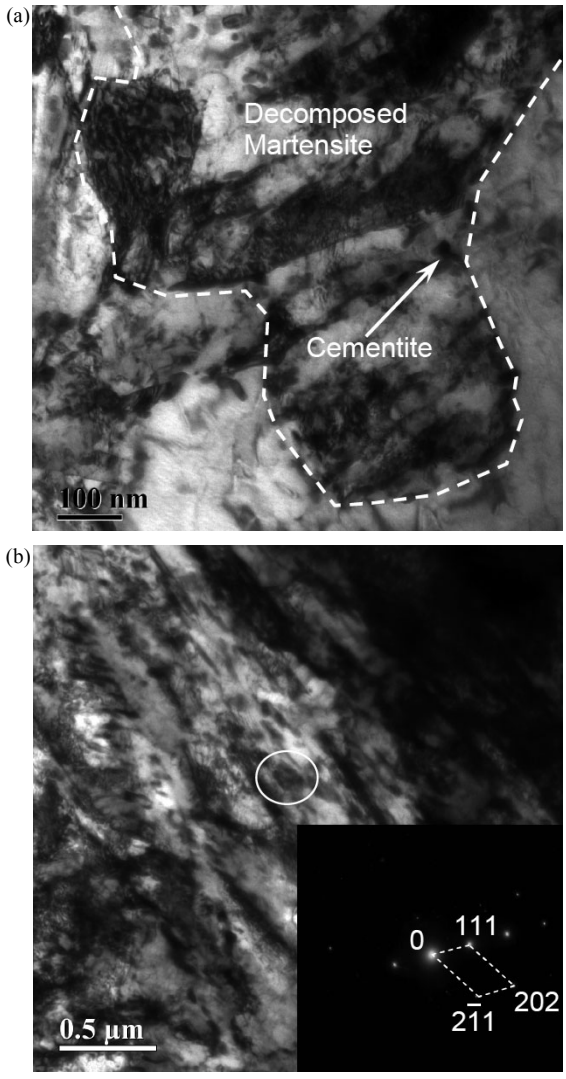


**Fig. 13.** DP780 heat treated in the Gleeble at 650°C for 0.5 s showing (a) the decomposed microstructure (b) an area with large carbides along with the SAD pattern of the carbides found in the decomposed martensite.

ture was eliminated. These observations coincide with those of Baltazar *et al*.[22] who saw similar changes in martensite and carbide morphology and location as well as the observed changes in ferrite dislocation structure. The microstructural analysis emphasised two conclusions. Primarily, although the Gleeble was not fast enough to reproduce the tempering response seen in welds made with very low heat input, it is believed that all of the samples underwent the same reaction path, regardless of whether tempering occurred during the isothermal Gleeble tempering or during the non-isothermal welding cycle. Furthermore, the microstructural changes reveal the complex metallurgical and mechanical changes responsible for the observed softening. This reinforces the earlier statement that the apparent activation energy and n parameters in the present JMAK form describing the process kinetics are a combination of a number of underlying processes. Thus, it should not be surprising that the values for Q and n derived in the present work differ from those expected.

## 4. Conclusions

Rapid isothermal tempering was performed on four dual-phase (DP) and three martensitic steels to characterise their tempering characteristics. The material's post-tempered hardness values were measured and modelled with the JMAK equation. The results of the isothermal tempering treatments were compared to hardness measurements and microstructural observations from welds to determine if this technique may be used to model the non-isothermal tempering that occurs in the sub-critical weld HAZ. From this study the following conclusions were drawn:

(1) Gleeble isothermal rapid tempering can produce a tempering response that allows the effects of time and temperature on tempering to be separated.

(2) The change in hardness from rapid iso-thermal tempering could be modelled using the JMAK equation with the effects of temperature accounted for by the Arrhenius equation.

(3) The activation energy for softening did not match the literature values for stage III tempering measured from dilatometry experiments, but did match literature values from hardness experiments. It is suspected that JMAK parameters derived from the changes in the hardness after isothermal rapid tempering characterised several complex metallurgical and mechanical changes within the samples, and could not be attributed to any single process.

(4) The non-isothermal temperature history in welding can be converted to an equivalent isothermal temperature history using the activation energy derived from the isothermal tempering experiments.

(5) The maximum HAZ softening in welds made under a variety of conditions could be accurately predicted using the JMAK equation.

(6) The microstructural changes of the Gleeble and weld tempered samples followed the same progression and matched observations seen in the literature. However, the Gleeble was not capable of the very low heat input/high temperature tempering possible in welding. Even though this low heat input regime could not be reproduced, it is believed that the Gleeble can accurately reproduce the tempering reaction seen in the sub-critical HAZ.

**Aknowledgements**

The authors would like to acknowledge Olivier Bouaziz, Patrick Barges, and Colin Scott from ArcelorMittal Global R&D Maizières, Annick Willems from OCAS as well as Dr. Sashank Nayak from the Centre for Advanced Materials Joining at the University of Waterloo for their input and guidance. Furthermore we would like to thank ArcelorMittal for granting us permission to publish this work.

## REFERENCES

1) *Federal Register*, **74** (2009), 49454.
2) W. Gan, S. S. Babu, N. Kapustraka and R. H. Wagoner: *Metall. Mater. Trans. A*, **37A** (2006), 3221.
3) R. G. Davies: *Metall. Trans. A*, **9A** (1978), 671.
4) J. Gerbase, J. D. Embury and R. M. Hobbs: Structure and Properties of Dual-Phase Steels, ed. by R. A. Kot and J. W. Morris, Metallurgical Society of the AIME, Warrendale, PA, (1979), 118.
5) D. K. Matlock, F. Zia-Ebrahimi and G. Krauss: Deformation, Processing, and Structure, ed. by G. Krauss, American Society for Metals, Metals Park, OH, (1982), 47.
6) R. G. Davies: Fundimentals of Dual-Phase Steels, ed. by R. A. Kot and B. L. Bramfitt, Metallurgical Society of the AIME, Warrendale, PA, (1981), 265.
7) N. Yamauchi, T. Taka, K. Kunishige and N. Nagao: *Trans. Iron Steel Inst. Jpn.*, **22** (1982), B-107.
8) T. Taka, K. Kunishige, N. Yamauchi and N. Nagao: *ISIJ Int.*, **29** (1989), 503.
9) M. Xia, E. Biro, Z. Tian and Y. N. Zhou: *ISIJ Int.*, **48** (2008), 809.
10) V. H. Baltazar Hernandez, S. K. Panda, Y. Okita and N. Y. Zhou: *J. Mater Sci.*, **45** (2010), 1638.
11) T. Waterschoot, K. Verbeken and B. C. De Cooman: *ISIJ Int.*, **46** (2006), 138.
12) E. Biro, J. R. McDermid, J. D. Embury and Y. Zhou: *Metall. Mater. Trans. A*, **41A**, (2010), 2348.
13) N. Yurioka, H. Suzuki and S. Ohshita: *Weld. J.*, **62** (1983), 147s.
14) T. Burns: Thesis, University of Waterloo, Ontario, Canada, (2010).
15) E-384-11e1 Standard Test Method for Knoop and Vickers Hardness of Materials, ASTM International, West Conshohocken, PA, (2011).
16) 18278-2 Resistance Welding–Weldability– Part 2: Alternative Procedures for the Assessment of Sheet Steels for Spot Welding, International Organization for Standardization, Geneva, (2004).
17) D. Rosenthal: *Weld. J.*, **20** (1941), 220 s.
18) W. A. Johnson and R. F. Mehl: *Trans. Am. Inst. Miner. Metall. Eng.*, **135** (1939), 416.
19) M. Avrami: *J. Chem. Phys.*, **7** (1939), 1103.
20) M. Avrami: *J. Chem. Phys.*, **8** (1940), 212.
21) M. Avrami: *J. Chem. Phys.*, **9** (1941), 177.
22) V. H. Baltazar Hernandez, S. S. Nayak and Y. Zhou: *Metall. Mater. Trans. A*, **42A** (2011), 3115.
23) J. C. Ion, K. E. Easterling and M. F. Ashby: *Acta Metall.*, **32** (1984), 1949.
24) R. W. Balluffi, M. Cohen and B. L. Averbach: *Trans. ASM*, **43** (1951), 497.
25) L. Cheng, C. M. Brakman, B. M. Korevaar and E. J. Mittemeijer: *Metall. Trans. A*, **19A** (1988), 2415.
26) E. J. Mittemeijer, L. Cheng, P. J. van der Schaaf, C. M. Brakman and B. M. Korevaar: *Metall. Trans. A*, **19A** (1988), 925.
27) T. Waterschoot K. Verbeken and B. C. De Cooman: *ISIJ Int.*, **46** (2006), 138.
28) M. Jung, S-J. Lee and Y-K. Lee: *Metall. Mater. Trans. A*, **40A** (2009), 551.
29) Y. Tomita: *Mater. Sci. Technol.*, **4** (1988), 977.
30) M. Takahashi and H. K. D. H. Bhadeshia: *Mater. Sci. Technol.*, **6** (1990), 592.
31) J. H. Hollomon and L. D. Jaffe: *Trans. Am. Inst. Miner. Metall. Eng.*, **162** (1945), 223.
32) J. W. Christian: Theory of Transformations in Metals and Alloys, Part I, Equilibrium and General Kinetic Theory, 2nd ed., Peregamon Press, Oxford, UK, (1975).